Unsaturated phospholipid modified FeOCl nanosheets for enhancing tumor ferroptosis

Zi He
College of Materials, Xiamen University
Yijun Guo
College of Materials, Xiamen University
Jinzhu Chen
College of Materials, Xiamen University
Huiling Luo
College of Materials, Xiamen University
Xinxin Liu
College of Materials, Xiamen University
Xiuming Zhang
College of Materials, Xiamen University
Yanan Sun
College of Materials, Xiamen University
Dongtao Ge
College of Materials, Xiamen University
Shefang Ye
Xiamen University
Wei Shi (shiwei@xmu.edu.cn)
Xiamen University

Research Article

Keywords: Ferroptosis, lipid peroxidation, FeOCl, Fenton reaction, lipid reactive oxygen species

Posted Date: July 6th, 2022

DOI: https://doi.org/10.21203/rs.3.rs-1786651/v1

Abstract

Iron-dependent accumulation of reactive oxygen species (ROS) and lipid peroxidation plays key roles in ferroptosis, which has been an attractive strategy to kill tumor cells. However, the rapid annihilation of hydroxyl radicals (•OH) produced by Fenton reaction has become a major obstacle to induce lipid peroxidation in cells. In this paper, we developed a nano delivery system of unsaturated phospholipid (Lip) and polyacrylic acid (PAA) functionalized FeOCl nanosheets (FeOCl@PAA-Lip). In this system, •OH produced by Fenton reaction between FeOCl nanosheets and endogenous H_2O_2 of tumor cells attacks Lip on the nanosheets *in situ* to initiate the lipid peroxidation chain reaction, which not only realizes free radical conversion but also achieves the amplification of ROS and lipid peroxides, thus enhancing tumor ferroptosis. The *in vitro* and *in vivo* results confirmed that FeOCl@PAA-Lip nanosheets exhibited specific tumor cell-killing effect, good biocompatibility, long circulation time, low side effects, high tumor targeting and excellent tumor inhibition rate (73%). The Lip functionalization strategy offers a paradigm of enhancing ferroptosis treatment by conversion of •OH/phospholipid radical/lipid peroxyl radical and strengthening lipid peroxidation.

Introduction

Ferroptosis, an iron-dependent non-apoptotic programmed cell death modality, has attracted remarkable attention as an emerging therapeutic target for cancer treatment[1–4]. It is widely accepted that the intracellular concentration of iron ion, reactive oxygen species (ROS) level and lipid peroxidation accumulation together construct the key factors affecting the ferroptosis of tumor cells[5–7].

In recent years, various iron-based nanotherapeutics, such as Fe_2O_3[8], Fe_3O_4[9, 10], FeOOH[11], FePt[12, 13], iron-based organic-framework[14] and amorphous iron[15], have been extensively studied for the inducing tumor ferroptosis. These iron-based nanotherapeutics produce lethal ROS through Fenton reaction with endogenous H_2O_2 of tumor cells, which leads to the accumulation of lipid peroxides (LPO) and realizes the specific tumor ferroptosis[16, 17]. Although the above nanotherapeutics activated ferroptosis of tumor cells and showed attractive application prospects in tumor therapy, it should be pointed out that most of the iron-based nanotherapeutics studied recently are spherical structures, and the iron source inside the spherical particles is difficult to participate in heterogeneous Fenton reaction, which leads to insufficient utilization of iron source. In addition, the harsh pH conditions of Fenton reaction restrict the catalytic efficiency in the tumor microenvironment (TME)[18, 19].

To solve the above problems, it is necessary to develop new iron-based materials to realize efficient Fenton reaction in TME[20]. Iron oxychloride (FeOCl), characterized by its self-stacked framework called “Van de Waals layer”, is a typical layered metal chloride oxide[21]. The large amount of space between layers of FeOCl enables it to catalyze H_2O_2 in a wide pH environment[22, 23]. In addition, the presence of unsaturated iron atoms on the surface of FeOCl plays a vital role in efficient catalytic process, allowing H_2O_2 to have more opportunities to convert to hydroxyl radical (•OH) by Fenton reaction[24]. Compared

with FeOCl plates, FeOCl nanosheets after exfoliation have larger surface and more active sites[25]. These excellent features make FeOCl nanosheets high catalysis reaction efficiency and utilization rate of iron source[26]. However, there are few reports on the application of FeOCl nanosheets in tumor ferroptosis[23].

Besides high Fenton reaction efficiency, strong LPO accumulation is also required for the tumor treatment based upon ferroptosis[27–29]. However, due to the extremely short lifetime of •OH (< 1 ns)[30], it can only attack the cell active components near its sites of generation by Fenton reaction in inducing tumor ferroptosis[31]. Therefore, many hydroxyl radicals have been annihilated before attacking the active components in the cell. The extremely low utilization of •OH makes it difficult to fully initiate lipid peroxidation in cells and has become a major bottleneck restricting the efficacy of ferroptosis.

Herein, we proposed a new strategy to enhance ferroptosis and fabricated an unsaturated phospholipid (Lip) and polyacrylic acid (PAA) functionalized FeOCl nanosheets (FeOCl@PAA-Lip) for inducing tumor ferroptosis, as shown in Scheme 1. After nanosheets internalization into tumor cells *via* endocytosis, FeOCl nanosheets reacted with H_2O_2 in tumor cells and produced •OH by Fenton reaction. The generated •OH would attack the unsaturated Lip on the FeOCl@PAA-Lip *in situ* and be converted into the phospholipid radical (L•) and lipid peroxyl radical (LOO•), which effectively avoid the annihilation of •OH. The generated L• and LOO• can not only oxidize unsaturated Lip on the nanosheets continuously, but also attack membranes of cells, mitochondria, lysosomes and nucleus to induce lipid peroxidation. Moreover, the lipid hydroperoxide (LOOH) generated in the chain reaction of lipid peroxidation can also be transformed into new LOO•, which would start a new round of lipid oxidation reaction and enhance the content of ROS in cells. These features ensure that the as-fabricated FeOCl@PAA-Lip achieved highly efficient ferroptosis both *in vitro* and *in vivo*.

Results And Discussion

Characterization of the FeOCl. Images of scanning electron microscopy (SEM) and transmission electron microscopy (TEM) (Fig. S1) of FeOCl plate we prepared displayed an irregular layered structure within nanoscale dimensions, which illustrates that it can be exfoliated by an appropriate method. To obtain FeOCl nanosheets with small particle size which meet the requirements of endocytosis of cells, acetonitrile was employed as exfoliating solvent, and FeOCl plates were dispersed in acetonitrile, followed by sonication in an ice water bath and in a water bath successively. After exfoliation, FeOCl appears as a slice layer structure with a diameter of about 30–80 nm (Fig. 1a) and a thickness of about 2.5–3.5 nm (Fig. 1c), which is apt to enter and accumulate in tumor cells. The structure of FeOCl before and after exfoliation is analyzed in X-ray diffraction (XRD) in Fig. S2. It can be seen that the diffraction peak of FeOCl plates before exfoliation is highly corresponded to the pure phase of orthogonalized FeOCl (standard card JCPDS, No.24-1005) in the plane of (010), (110) and (021), and there is no diffraction peak of other phase. After exfoliation, the disappearance of the diffraction peak in FeOCl nanosheets proved that the crystal structure of the original sample was destroyed, which further demonstrates the successful exfoliation of FeOCl plates. In order to clarify the change in iron ion valence upon exfoliation

of FeOCl, X-ray photoelectron spectroscopy (XPS) analysis was performed. As shown in Fig. S3, compared with the FeOCl plates, the binding energy of the Fe element in the FeOCl nanosheets shifts to a lower field, indicating that more Fe^{3+} has been transformed into Fe^{2+}, which is beneficial for the Fenton reaction. The iron ions release of FeOCl before and after exfoliation was investigated under various pH conditions as showed in Fig. S4. It is obviously observed that the release amount of iron ions in the exfoliated FeOCl nanosheets is significantly higher than that of FeOCl plates. The release of iron ions increased with the decrease of pH, and the amount of released iron ions of FeOCl nanosheets could reach up to 10% at pH 5.0, suggesting potential pH responsive release of iron ions in tumor microenvironment.

To enhance the stability, FeOCl nanosheets were modified with PAA and Lip. After coating PAA and Lip onto the FeOCl nanosheets, the lateral size of the nanosheets has not apparently changed (Fig. 1b), while the thickness increased to 5–6.5 nm (Fig. 1d). To confirm the association of PAA and Lip with the FeOCl nanosheets, Fourier transform infrared spectroscopy measurements were carried out. As shown in Fig. 1e, the FeOCl showed stretching vibration peaks of Fe-O bonds at 845 cm^{-1} and 684 cm^{-1}, and the appearance of -COOH peaks at 2924 cm^{-1} and 2853 cm^{-1} in FeOCl@PAA proved the successful modification of PAA. In addition, the peaks at 1737.5 cm^{-1} and 1246 cm^{-1} are attributed to the peak of C = O in Lip and the peak of -CH_2 in polyethylene glycol (DSPE-PEG), confirming the coating of Lip and DSPE-PEG. Dynamic light scattering (DLS) was used to characterize size and zeta potential of modified samples. FeOCl showed hydrodynamic particles size of 58 nm (polydispersity index (PDI) = 0.21) and a zeta potential of + 36 mV (Fig. 1f and g). After modification of PAA and Lip, the size of the nanosheets was enlarged to 68 nm (PDI = 0.18) and 78 nm (PDI = 0.20), and the zeta potential was transformational to -33 mV and − 21 mV, respectively. The FeOCl@PAA and FeOCl@PAA-Lip can be well dispersed in water, PBS and cell culture medium, indicating excellent physiological stability (Fig. 1h).

ROS detection

The production of •OH is significant for inducing ferroptosis of tumor cells, so we first examined the generation of •OH. The •OH can be captured by 5,5-dimethyl-1-pyrroline N-oxide (DMPO), and detected by an electron spin resonance (ESR) instrument[32]. The clear ESR signals with intensity ratio of 1:2:2:1 were observed for all samples at pH 7.4, indicating that FeOCl nanosheets can generate •OH in neutral (Fig. 2a and Fig. S5). To further verify the results, terephthalic acid (TA) was used as a chemical probe to measure the generation of •OH of the nanosheets. TA reacts with •OH to form a fluorescent product, 2-hydroxyterephthalic acid (TAOH), which could be excited by 325 nm light and produced emission at 426 nm. Figure 2b and Fig. S6 showed the fluorescence spectra of TA in H_2O_2 and FeOCl nanosheet solutions at wide pH values (pH 5.0-7.4). Compared with the control group, the significantly increased fluorescence intensity at pH 7.4 indicates that the FeOCl nanosheets could catalyze H_2O_2 into •OH under mild acidic TME. Both the ESR spectrum and TA probe method showed that FeOCl nanosheets produced •OH well at neutral pH, which overcomes the harsh pH requirements of traditional Fenton reaction and is conducive to the wider application of tumor treatment based upon ferroptosis. Moreover, the •OH level in the solutions containing FeOCl nanosheets was found gradually enhanced as the pH value of solution

decreased (Fig. S5 and S6). The results demonstrated that an acid environment, such as the tumor acidic microenvironment (pH 5.0 ~ 6.5), could facilitate the generation of •OH *via* the Fenton reaction between H_2O_2 and FeOCl nanosheets. To explore the effect of H_2O_2 on the Fenton reaction of FeOCl@PAA and FeOCl@PAA-Lip, methylene blue (MB) degradation test was carried out. MB is easy to be oxidized and degraded by •OH to produce colorless products and this process can be tracked by measuring the variation of absorbance at 660 nm with UV-vis spectrophotometer (Fig. 2c and Fig. S7). Compared with the control group, the maximum absorption of MB gradually decreased with the increase of H_2O_2 concentration, indicating that higher concentration of H_2O_2 contributes to Fenton reaction and the production of •OH.

It should be pointed out that the detected •OH level of FeOCl@PAA-Lip was significantly lower than that of the FeOCl and FeOCl@PAA nanosheets in all the above •OH tests, including ESR spectrum, TA probe and MB degradation. To explore whether •OH produced by Fenton reaction between the FeOCl nanosheets and H_2O_2 was consumed by Lip, the content of LPO was measured by xylenol orange color method. LPO oxidize Fe (II) to Fe (III), which can combine with yellow xylenol orange to produce red-purple complex with a characteristic absorption peak at about 580 nm. As shown in Fig. 2d, there is no absorption peak at 580 nm in the FeOCl@PAA group, whether H_2O_2 is present or not. However, for the FeOCl@PAA-Lip group, an obvious characteristic peak of LPO was observed in the presence of H_2O_2, indicating that •OH produced by Fenton reaction attacks Lip to produce LPO. These results suggested that the Lip on the FeOCl@PAA-Lip could convert •OH with short half-life into stable LPO *in situ*, which not only avoided quick annihilation of •OH but also enhanced the spreading of the lipid peroxidation chain reaction.

Detection of intracellular ROS and Malondialdehyde. The fluorescent-free 2',7'-dichlorodihydrofluorescein diacetate (DCFH-DA) can be oxidized by ROS to generate fluorescent 2',7'-dichloro-fluorescein (DCF), which is widely used as fluorescent probe to detect intracellular ROS, such as •OH, LOO• and L•. To test the cellular ROS of FeOCl@PAA and FeOCl@PAA-Lip, DCFH-DA was utilized to measure the ROS production in 4T1 cells. As shown in Fig. 3a, the fluorescence intensity increased with incubation time and FeOCl@PAA-Lip showed obvious green fluorescence after 6 h. The FeOCl@PAA-Lip treated 4T1 cells exhibited stronger fluorescence intensity than that of FeOCl@PAA. The results of flow cytometry were consistent with those of confocal laser scanning microscopy (CLSM) observations, and the ROS generation of 4T1 cells incubated with FeOCl@PAA-Lip was 2.8 times as that of FeOCl@PAA (Fig. 3b). This enhancement effect of ROS can be attributed to the chain reaction of lipid peroxidation initiated by Lip, as shown in Fig. 3c. •OH produced by Fenton reaction attacks Lip on the nanosheets *in situ* to form free radical intermediate, L•. The L• can reversibly convert to LOO• with the participation of molecular oxygen or Lip. The generated LOO• then reacts with Lip and forms LOOH and L•. LOOH can further generate new LOO• in the presence of Fe^{2+}. Therefore, the chain reaction of lipid peroxidation not only realizes free radical conversion but also achieves the amplification of ROS. Here, it needs to be additional emphasized that besides Lip on the nanosheets, the L• and LOO• generated from the above chain reaction of lipid peroxidation can also attack Lip on the membranes of cells, mitochondria, lysosomes and

nucleus to induce lipid peroxidation[33], which would expand lipid peroxidation and enhance ferroptosis of tumor cells.

Ferroptosis lethality depends on the iron-dependent accumulation of LPO[34]. To investigate whether the chain reaction of lipid peroxidation takes place in the tumor cells internalized with FeOCl@PAA-Lip, we analyzed the content of the end product of LPO, malondialdehyde (MDA). As shown in Fig. 3d, the 4T1 cells treated with FeOCl@PAA-Lip showed about 1.35-fold MDA accumulation as that treated with FeOCl@PAA, implying that Lip on the nanosheets can significantly enhance the chain reaction of lipid peroxidation, which helps to strengthen the ferroptosis of tumor cells.

Cell cytotoxicity. Cytotoxicity is a key indicator of therapeutic agent for *in vivo* antitumor treatment. The potential cytotoxicity of FeOCl@PAA and FeOCl@PAA-Lip was tested using mouse fibroblast L929 cells (L929). It was found that FeOCl@PAA and FeOCl@PAA-Lip exhibited negligible cytotoxicity toward normal cells. As shown in Fig. 4a, the cell viability was still higher than 90% even with the treatment of 300 μg/mL FeOCl@PAA and FeOCl@PAA-Lip after 48 h. However, concentration-dependent cytotoxicity was observed in mouse breast cancer 4T1 cells (4T1) and Human malignant glioma U87 cells (U87) (Fig. 4b and c). The viabilities of 4T1 cells and U87 cells cultured with 300 μg/mL FeOCl@PAA for 48 h were 82.7% and 69%, respectively. At the same incubation concentration, the cell viabilities of 4T1 cells and U87 cells incubated with FeOCl@PAA-Lip were decreased to 59% and 47.4%, respectively. Compared with FeOCl@PAA, the FeOCl@PAA-Lip displayed higher cytotoxicity to tumor cells. It is mainly because Lip realized free radical conversion and promoted the accumulation of LPO. To further investigate the cell cytotoxicity of the nanosheets, the flow cytometric analysis was utilized by staining 4T1 cells with annexin V-FITC and propidium iodide (PI). As shown in Fig. 4g, compared with FeOCl@PAA, FeOCl@PAA-Lip induced an obviously higher ferroptosis rate (62.7%), which could be credited to the high level of ROS and LPO. In addition, the cytotoxic effect of nanosheets was specific to tumor cells but minimal for normal cells, which is due to the abundant H_2O_2 in tumor cells.

In order to evaluate the cell cytotoxicity of FeOCl@PAA and FeOCl@PAA-Lip in a more realistic tumor environment, the cell viability was investigated *via* additional H_2O_2 supplement in cell culture. As shown in Fig. 4d and e, the greater cytotoxicity of 4T1 was dependent on the higher H_2O_2 concentration. The same phenomena were observed in U87 cells treated with FeOCl@PAA and FeOCl@PAA-Lip containing 300 μM H_2O_2 (Fig. 4f). FeOCl@PAA-Lip showed a particularly striking decline in cell activity, which was mainly attributed to the abundant H_2O_2 unbalanced the antioxidant system of 4T1 cells and promoted the Fenton reaction. Flow cytometry results (Fig. 4g) showed that cell viability decreased to 34.6% and 15.5% under treatment with FeOCl@PAA and FeOCl@PAA-Lip containing 300 μM H_2O_2, respectively. The facilitation of H_2O_2 was then further assessed using fluorescence microscopic imaging after co-staining 4T1 cells with calein acetoxymethylester (AM) and propidium iodide (PI), with live cells in green and dead cells in red (Fig. S8). In comparison with cells without additional H_2O_2 supplement, the 4T1 cells added with 300 μM H_2O_2 displayed remarkably enhanced red fluorescence, directly indicating higher ferroptosis, which was in agreement with the MTT and flow cytometry analyses. In addition, the cancer cells showed

lower activity after incubation 48 h than 24 h, due to the accumulation of ROS and the more release of Fe ions for enhancement of Fenton reaction. These results suggested that the introduction of Lip was an effective means to enhance ferroptosis effect.

In Vitro **Ferroptosis Mechanism.** Ferroptosis, a type of programmed cell death, can be triggered by glutathione (GSH) depletion, GPX4 deactivation and the iron-dependent accumulation of lipid reactive oxygen species and lipid peroxidation products[35]. The established ferroptosis mechanism induced by FeOCl@PAA-Lip and ferroptosis-related compounds was shown in Fig. 5a. GPX4 protects cells against peroxidation of lipids caused by ROS, and uses GSH as a substrate. However, additional glutamic acid (Glu) causes the inhibition of system X_c^-, which mediates transportation of cystine into cells in ferroptosis upstream. This inhibition prevents the biosynthesis of GSH and GPX4, which leads to the accumulation of ROS and LPO that are lethal to the cells. It was found that preventing lipid peroxidation and removing intracellular oxidative environment by inhibitor of ferroptosis Ferrostatin-1 (Fer-1), Vitamin C (VC) and Vitamin E (VE) (the lipophilic antioxidants) can block ferroptosis[36]. In addition, releasing sufficient amount of Fe ion is the key step to ferroptosis by Fenton reaction. Reducing the available intracellular Fe ion content by iron chelators deferoxamine (DFO) is another way to prevent ferroptosis. Therefore, the viability of 4T1 cells treated with ferroptosis inducer Glu and ferroptosis inhibitors DFO, GSH, Fer-1, VC and VE were studied to confirm that the cell death mechanism of FeOCl@PAA-Lip treated cancer cells was ferroptosis (Fig. 5b). The introduction of ferroptosis inhibitors, especially Fer-1 and GSH, both substantially reduced the cell-killing effect of FeOCl@PAA and FeOCl@PAA-Lip. On the contrary, the cell activity was significantly reduced when Glu was added due to the inhibition of cysteine supply, which further leads to GSH deficiency. These results indicated that the mechanism of 4T1 cell death treated with FeOCl@PAA and FeOCl@PAA-Lip was ferroptosis by Fenton reaction and lipid peroxidation.

In Vivo **Antitumor Efficacy.** 4T1 tumor-bearing mice were used to establish antitumor model to explore the curative effect of the nanosheets *in vivo*. When the tumor volume reached 50 mm^3, the mice were divided randomly into three groups and treated with PBS solution, FeOCl@PAA or FeOCl@PAA-Lip, respectively. To evaluate the antitumor efficacy, the relative tumor size, body weight and H&E stained images of different groups were recorded. As shown in Fig. 6a, compared with PBS group, the tumor volume after the treatment of FeOCl@PAA and FeOCl@PAA-Lip exhibited significantly inhibition, due to the ROS accumulation by Fenton reaction mediated ferroptosis. FeOCl@PAA-Lip group could more efficiently inhibit the tumor growth and the tumor inhibition rate could reach 73.3%. This result demonstrated once again that the Lip on the FeOCl@PAA-Lip enhanced ferroptosis by lipid peroxidation chain reaction and the amplification of ROS. The photographs of mice in all three groups on different days (Fig. 6b) and collected tumors after 14 days (Fig. 6c) were in line with tumor growth curves. H&E staining was utilized to further explore the therapeutic effects of various treatments. As shown in Fig. 6d, the morphology of most tumor cells treated with PBS group remained intact. However, the tumor slices from the FeOCl@PAA-Lip group showed more significant killing effect on tumor cells by presenting cancer cells with deformed nucleus (karyorrhexis and karyolysis) than that from FeOCl@PAA group. The result reproved the excellent ferroptosis effect of FeOCl@PAA-Lip *in vivo*.

In vivo **biosafety and biodistribution evaluation.** To investigate the blood compatibility of FeOCl@PAA-Lip, the hemolysis test in fresh blood was performed (Fig. 7a). The hemolysis ratio was less than 2% even with the treatment of 300 μg/mL FeOCl@PAA-Lip after 24 h, demonstrating the good biocompatibility. To further explore *in vivo* safety profile, a series of blood biochemical indicators of mice treated with PBS, FeOCl@PAA and FeOCl@PAA-Lip after 7 days were tested (Fig. S9). Compared with the PBS group, the blood biochemistry indexes were all within the normal reference ranges, indicating that no obvious toxicity on liver and kidney functions within 7 days. Moreover, no significant change of body weight was found during the whole experiment (Fig. 6e). As shown in Fig. S10, there was no obvious pathologic abnormality in major organs including heart, liver, spleen, lung and kidney after different treatments by H&E staining, indicating minor side effects of FeOCl@PAA and FeOCl@PAA-Lip mediated ferroptotic therapy.

To observe biodistribution of the nanosheets, we labeled FeOCl@PAA-Lip with fluorescent dyes Cy 5.5. A large amount of fluorescence appeared in the kidney of both Cy 5.5 and Cy 5.5/FeOCl@PAA-Lip group in the initial period after intravenous injection (Fig. 7b). The fluorescence of Cy 5.5 group gradually decreased after 3 h, and then almost was removed through metabolism in the body after 36 h. On the contrary, the fluorescence signal of Cy5.5/FeOCl@PAA-Lip at tumor site increased gradually and reached maximum at 24 h, indicating that FeOCl@PAA-Lip could accumulate in tumor. The long cycle time can also be derived from the stable fluorescence intensity at the tumor site after 36 h and 48 h, which could be ascribed to the relatively small size of the nanoparticles (30～80 nm) and Lip modification. The iron content in different organs was measured using ICP-MS to further quantify accumulation of FeOCl@PAA-Lip in tumor. As shown in Fig. 7c, FeOCl@PAA-Lip group showed the high iron content of the *ex vivo* tumor harvested from mice after 24 h, which was 1.31-folds of FeOCl@PAA group, demonstrating the enhanced EPR effect due to Lip modification. Based on above results, the preeminent characteristic of FeOCl@PAA-Lip with remarkable stability and excellent EPR toward tumor endowed it potential applications *in vivo* as a theranostic agent.

Conclusions

FeOCl nanosheets with high Fenton reaction efficiency at neutral pH values (pH 6–7) were prepared by exfoliating FeOCl plate. After modified with Lip and PAA, a nano delivery system based on inducing tumor ferroptosis, FeOCl@PAA-Lip nanosheets were fabricated. The Lip on the nanosheets could not only convert •OH generated from Fenton reaction between FeOCl and H_2O_2 into L• and LOO• *in situ*, avoiding the annihilation of •OH, but also participate in lipid peroxidation chain reaction with membranes of cells, mitochondria, lysosomes and nucleus, enhancing the level of ROS in cells and amplifying ferroptosis effect. Moreover, FeOCl@PAA-Lip nanosheets exhibited good passive targeting to tumor, excellent biocompatibility as well as blood compatibility, and low side effects. These outstanding features of FeOCl@PAA-Lip nanosheet are expected to make it a powerful platform for inducing tumor ferroptosis.

Experiment Section

Materials. Soya bean lecithin (Lip) was obtained from Sinopharm group chemical reagent Co., Ltd. 1,2-distearoyl-sn-glycero-3-phosphatidylethanolamine (DSPE-PEG) and Iron (III) chloride hexahydrate ($FeCl_3·6H_2O$) was supplied by Xiamen Sinobang Biological Technology Co., Ltd. Polyacrylic acid (PAA, 50 wt% in H_2O, Mw ~ 50,000), DCFH-DA, Glu, cystine (Cys) were bought from Sigma-Aldrich. DFO, GSH and VE was purchased from Mitsubishi Chemical Corporation. Dulbecco's modified Eagle's medium (DMEM), Roswell Park Memorial Institute (RPMI) 1640 medium and fetal calf serum (FBS) were acquired from Life Technologies Co., Ltd. All solvents and reagents were obtained commercially.

Synthesis and exfoliation of FeOCl plates. FeOCl plates were obtained by a solid-phase method. The polished $FeCl_3·6H_2O$ was tiled into the bottom of 5 mL crucible and covered for reaction for 1 h in a high-temperature oven (240°C, the heating rate was 10°C per minute). After cooling to room temperature, FeOCl plates were fully ground until there was no agglomeration, and cleaned with a large amount of anhydrous acetone to remove the unreacted $FeCl_3·6H_2O$, then dried overnight in a vacuum oven (90°C).

Exfoliation of the FeOCl plates was performed by dispersing the FeOCl plates (30 mg) in acetonitrile (30 mL). The suspensions were broken by sonication in an ice water bath for 3 h (500 W, 5 s/5 s), and in a water bath for 48 h (37°C, 480 W). The supernatant was collection after 10 min of centrifugation at 8000 rpm, and then nanosheets were gathered by centrifugation at 13000 rpm for 20 min.

Modification of nanosheets. 3 mL PAA (10 mg/mL) were added dropwise into 30 mL FeOCl nanosheets solution (1 mg/mL) under magnetic stirring. After 5 h, FeOCl@PAA nanosheets were gathered by centrifugation (13000 rpm, 20 min) and then washed for 3 times by water. FeOCl@PAA, Lip and DSPE-PEG were mixed with the mass ratio of 1:1:1 and stirred 24 h. Finally, the obtained product (FeOCl@PAA-Lip) was stored in water at 4°C after centrifugation (13000 rpm, 20 min) and washing by water for 3 times.

Characterization. X-ray diffraction (XRD) analysis was carried out on a 2.2 kW X-ray diffractometer using Cu (60 kV, 55 mA) radiation. SEM and TEM images were obtained by a Hitachi S4800 and a JEOL JEM-1400, respectively. A SHIMADZU UV-1750 spectrophotometer and a Nicolet iS10 FTIR spectrometer were used for UV-vis-NIR spectra and Fourier transform infrared (FTIR) spectra, respectively. The size and zeta potential of products were measured by Malvern Zeta sizer Nano ZS (model: ZEN 3600). The concentration of iron ion was determined by -an inductively coupled plasma mass spectrometry (ICP-MS, Agilent 7500ce) Confocal fluorescence images were recorded by Olympus FV1000 laser scanning confocal microscopy. Atomic force microscope (AFM, Multimode 8) was used to determine the thickness of the nanosheets.

Release of Fe. 1 mL 50 μg/mL FeOCl before and after exfoliation was added into dialysis membrane (6000 Da), respectively, and incubated in 20 mL PBS solution (pH 7.4 or pH 5.0) under shaking at 37°C (100 rpm). At pre-determined time intervals, 1 mL dialysate was extracted for analysis by ICP, and 1mL corresponding fresh medium was replenished into remaining dialysate.

Detection of ·OH and LPO. To compare the ·OH generation ability of FeOCl@PAA and FeOCl@PAA-Lip under different pH, colorimetric method was employed based on the oxidation of TA. More precisely, 300 μL sample solution (200 μg/mL), 300 μL H_2O_2 aqueous solution (10 mM) and 300 μL TA (5 mM) was transferred into 2.1 mL PBS (pH = 7.4, 6.5, 5.0). The mixture was tested under 435 nm excitation light after shaking 12 h at 37°C in the dark. In addition, MB was exploited to detect the ROS production of FeOCl@PAA and FeOCl@PAA-Lip under various H_2O_2 concentrations. 2 mL sample solution (250 μg/mL) and 1 mL MB (30 mg/L) were respectively added into 2 mL H_2O_2 aqueous solution (0, 1, 5, 10, 20 mM) and then the mixture was kept at 37°C for 12 h. After centrifugation (10000 rpm, 10 min), the absorbance value of MB at 665 nm was detected.

Xylenol orange method was used to test the production of LPO. 100 μg/mL FeOCl@PAA (with/without 10 mM H_2O_2), 100 μg/mL FeOCl@PAA-Lip (with/without 10 mM H_2O_2) and xylenol orange were placed in a constant temperature shaker at 37°C for 24 h, followed by dialysis (100 Da) to remove excess H_2O_2 and iron ions for another 48 h with changing water frequently. 1 M H_2SO_4 was used to adjust the pH of sample to less than pH 6.5 after dialysis. 5 mL sample was added into 100 μL detection solution (0.3 mM $FeSO_4$, 20 mM H_2SO_4 and 150 μM xylenol orange), followed by reacting in a 30°C water bath for 30 min. The supernatant was collection for further test after centrifugation.

Cell culture. 4T1 murine breast cancer cells, U87 human glioma cells and L929 mouse fibroblast cells were incubated in RMPI 1640 medium containing 10% FBS at 37°C in a humidified atmosphere containing 5% CO_2.

In vitro **cell toxicity test.** MTT assay was used to evaluated the *in vitro* cytotoxicity. L929, 4T1 and U87 cells were seeded into 96-well plates (1×10^4 per well) and incubated 24 h. Then, 200 μL fresh medium (with or without H_2O_2) containing different concentrations of FeOCl@PAA or FeOCl@PAA-Lip nanosheets were co-incubated with cells for 24 h or 48 h. After co-incubation, the cells were washed with PBS and treated by 100 μL of 10% MTT solution in each well for 4 h. After that, the MTT solution was replaced by 200 μL DMSO for 30 min. Finally, the absorbance at 570 nm was measured by a microplate reader (TECAN, infinite M200 PRO).

For flow cytometric analysis, 1 mL cell suspension (1×10^5 cells) were cultured with FeOCl@PAA, FeOCl@PAA-Lip, FeOCl@PAA + H_2O_2 and FeOCl@PAA-Lip + H_2O_2 for 24 h, respectively. The cells were collected by centrifugation and washing by PBS. Diluted Annexin V-FITC and PI solutions were added successively to stain the cells, and then these cells were analyzed using a flow cytometry () (MoFlo, XDP, USA).

For calcien AM/PI staining observation, 500 μL 4T1 cells (1×10^4/mL) were plated for 12 h in culture dishes with a diameter of 6 cm, then the medium was replaced by 500 μL medium (with or without H_2O_2) containing different concentrations of FeOCl@PAA or FeOCl@PAA-Lip for 24 h. 5 μL PI (16 mM) and 5 μL

AM (4 mM) were added into 10 mL PBS. After washing by PBS, 1 mL above calcien AM/PI solution was used to stain cells for 30 min at 37°C, followed by fluorescent microscope observation.

In vitro **ROS detection.** Confocal laser scanning microscopy (CLSM) was used to observe the levels of ROS in 4T1 cells. 5×10^4 4T1 cells were seeded onto a round coverslip. After attachment the cells were cultured for 12 h in a 24-well plate, followed by treating with the medium containing 300 μg/mL FeOCl@PAA or FeOCl@PAA-Lip nanosheets and 0.3 mM H_2O_2 for 2, 4 or 6 h. After being washed by PBS, 200 μL of 10 μM DCFH-DA was added, and the cells were further cultured for 20 min to measure the generation of ROS. Hoechest 33258 dye was utilized for nuclear staining. The fluorescent signal of DCF and Hoechest 33258 was tested by CLSM.

A MDA assay kit was utilized to measure the intracellular LPO content. 1×10^6 cells per well were seeded into 6-well plates and then incubated with 500 μg/mL FeOCl@PAA and FeOCl@PAA-Lip for 12 h respectively. Cell suspension was obtained by repeated blowing, and then supernatant was discarded after centrifugation to collect cell precipitation. 1 mL MDA extract was added to the cell precipitation, and an ultrasonic crusher was used (200 W, 3 s on/10 s off, 7 min) for crushing. The supernatant was obtained after centrifugation (8500 rpm, 4°C, 10 min), followed by adding working fluid to the supernatant according to the MDA test kit and keeping at 100°C for 1 h. The supernatant was collected by centrifugation, followed by measuring the absorbance of above supernatant at 450 nm, 532 nm and 600 nm *via* microplate reader. Intracellular MDA content was calculated according to the specification of the kit instructions.

For ferroptosis mechanism analysis, 4T1 cells were seeded in 96-well plates at a density of 1×10^4 cells per well and cultured for 12 h. FeOCl@PAA or FeOCl@PAA-Lip was added into each well, and then immediately added media with 10 mM DFO, 1 μM Fer-1, 5 mM GSH, 2 mM Glu, 100 μM VC and 100 μM VE, respectively. The cells were then co-incubated for 24 h, followed detecting cell viability using MTT assay.

Animal model building. Female BALB/c mice (4 – 6 weeks old) were purchased from Xiamen University Laboratory Animal Center and used in accordance with the guidelines of the Chinese National Science and Technology Committee. BALB/c tumor-bearing mice models were established by subcutaneous injecting of 100 μL 4T1 tumor cells (1×10^8 cells) into the flank of mice. Further experiments were performed when the tumor volume increased to 50 mm^3.

In vivo **imaging.** To observe the distribution of the nanosheets *in vivo*, fluorochrome Cy 5.5 was loaded onto FeOCl@PAA-Lip nanosheets. Two female Balb/c mice with tumor volume of about 200 mm^3 were injected with 200 μL of Cy 5.5-labeled FeOCl@PAA-Lip and free Cy 5.5 into the tail vein with a dose of 20 mg/kg, respectively. The whole-body fluorescence imaging pictures were taken at 1, 3, 5, 7, 9, 11, 24, 36, and 48 h after injection by the mouse optical imaging system (parameter: Ex 630 nm, Em 645–680 nm).

In vivo **therapy.** Eighteen female Balb/c mice with tumor volume of about 50 mm^3 were divided into three groups at random: control group (PBS injection), the FeOCl@PAA group and the FeOCl@PAA-Lip group. The tumor-bearing mice were treated with different medicament (200 μL) by injecting *via* the tail vein with a dose of 20 mg/kg on the 0, 1, 3, 5, 7, 9, 12th day. The tumor volume and weight of mice were continuously measured and photos were taken once a week. After treatment for 14 days, tumor of each mouse was stripped and taken pictures. At the same time, the major organs, including heart, liver, spleen, lung, and kidney, were dissected and fixed with 4% glutaraldehyde solution, dehydrated with alcohol, embedded in paraffin and stained with H&E and observed.

Determination of iron content in living animal organs. After injecting PBS, FeOCl@PAA and the FeOCl@PAA-Lip for 24 hours, 3 mice were taken from each group and each mouse was dissected to get the heart, liver, spleen, lung, kidney and tumor for weighing. Then, nitric acid was used to nitrolysis all organizations. After the tissue is completely oxidized and nitrified, digestion solution was diluted (concentration of nitric acid < 5%), followed by filtration with a 0.22 μm microporous filter membrane for ICP-MS testing. The iron content of each organ is calculated based on the wet weight and the ICP-MS data.

Hemolysis experiment. Blood was taken by extracting the eyeballs from three healthy female Balb/c mice, and centrifuged at 4°C at 2000 rpm for 5 min to separate red blood cells. 200 μL erythrocyte suspension were mixed with 800 μL of deionized water (positive control), PBS pH 7.4 (negative control) and FeOCl@PAA-Lip PBS solutions with various concentrations (25, 50, 100, 200, 300, and 500 μg/mL), respectively. After culturing at 37°C for 24 h, centrifugation was implemented (2000 rpm, 5 min, 4°C), followed by testing the absorbance with a multifunctional microplate reader at 541 nm. The hemolysis percentage is calculated as follows:

$$x = \frac{A_S - A_{C(-)}}{A_{C(+)} - A_{C(-)}} \times 100\%$$

Among them, A_S, $A_{C(-)}$ and $A_{C(+)}$ represent the absorbance of the experimental group containing FeOCl@PAA-Lip, the negative control group containing PBS and the positive control group containing deionized water, respectively.

Analysis of blood biochemical indexes. Blood was taken from the eyeball of twelve female Balb/c mice received different treatment (PBS group, FeOCl@PAA group and FeOCl@PAA-Lip group) after therapy for one week, then centrifuged at 2000 rpm for 5 min at 4°C. The supernatant plasma was carefully aspirated and tested the content of aspartate aminotransferase (AST), alanine aminotransferase (ALT), alkaline phosphatase (ALP), urinary nitrogen (BUN) and creatinine (CRE) content.

Declarations

Ethics approval and consent to participate

All animal experimental procedures were approved by the Care and Use Committee of Xiamen University.

Consent for publication

All authors have approved the final draft of this manuscript for submission and have given consent for the publication of identifiable details.

Availability of data and materials

The authors agree to share data and materials related to this manuscript.

Competing interests

The authors declare no competing financial interest.

Funding

This work was supported by the National Natural Science Foundation of China (22172132, 31870986, 31271009, 32071396), the Natural Science Foundation of Fujian Province of China (2021J01041, 2020J01036) and the Program for New Century Excellent Talents in University.

Authors' contributions

Conceptualization: WS and DG; Methodology: ZH, YG, JC, HL, XL, WS, YS, SY and DG; Investigation: ZH, YG, XZ and SY; Data analysis: ZH, YG, JC and SY; Writing- Original Draft: ZH and YG; Writing-Review & Editing: ZH, YG, WS, SY and DG; Funding Acquisition: WS, YS and SY; Supervision: WS, SY and DG. All authors reviewed the manuscript.

Acknowledgements

Not applicable.

Authors' information

The Higher Educational Key Laboratory for Biomedical Engineering of Fujian Province/Research Center of Biomedical Engineering of Xiamen, Department of Biomaterials, College of Materials, Xiamen University, Xiamen, 361005, China

References

1. Stockwell BR, Angeli JPF, Bayir H, Bush AI, Conrad M, Dixon SJ, et al. Ferroptosis: A Regulated Cell Death Nexus Linking Metabolism, Redox Biology, and Disease. Cell 2017; 171: 273–285.
2. Sun LL, Linghu DL, Hung MC. Ferroptosis: A Promising Target for Cancer Immunotherapy. Am. J. Cancer Res. 2021; 11: 5856–5863.

3. Shan X, Li S, Sun B, Chen Q, Sun J, He Z, et al. Ferroptosis-Driven Nanotherapeutics for Cancer Treatment. J. Control. Release 2020; 319: 322–332.
4. Shen Z, Song J, Yung BC, Zhou Z, Wu A, Chen X. Emerging Strategies of Cancer Therapy Based on Ferroptosis. Adv. Mater. 2018; 30: 1704007.
5. Yang WS, SriRamaratnam R, Welsch ME, Shimada K, Skouta R, Viswanathan V, et al. Regulation of Ferroptotic Cancer Cell Death by GPX4. Cell 2014; 156: 317–331.
6. Dixon SJ, Stockwell BR. The Role of Iron and Reactive Oxygen Species in Cell Death. Nat. Chem. Biol. 2014; 10: 9–17.
7. Shen Z, Liu T, Li Y, Lau J, Yang Z, Fan W, et al. Fenton-Reaction-Acceleratable Magnetic Nanoparticles for Ferroptosis Therapy of Orthotopic Brain Tumors. ACS Nano 2018; 12: 11355–11365.
8. Liu J, Chen H, Fu Y, Li X, Chen Y, Zhang H, et al. Fabrication of Multifunctional Ferric Oxide Nanoparticles for Tumor-Targeted Magnetic Resonance Imaging and Precise Photothermal Therapy with Magnetic Field Enhancement. J. Mater. Chem. B 2017; 5: 8554–8562.
9. Chen JX, Lei S, Zeng K, Wang MZ, Asif A, Ge XW. Catalase-Imprinted Fe_3O_4/Fe@Fibrous SiO_2/Polydopamine Nanoparticles: An Integrated Nanoplatform of Magnetic Targeting, Magnetic Resonance Imaging, and Dual-Mode Cancer Therapy. Nano Res. 2017; 10: 2351–2363.
10. Wang Y, Li H, Guo L, Jiang Q, Liu F. A Cobalt-Doped Iron Oxide Nanozyme as a Highly Active Peroxidase for Renal Tumor Catalytic Therapy. RSC Adv. 2019; 9: 18815–18822.
11. Zebrowska K, Coy E, Synoradzki K, Jurga S, Torruella P, Mrowczynski R. Facile and Controllable Growth of Beta-FeOOH Nanostructures on Polydopamine Spheres. J. Phys. Chem. B 2020; 124: 9456–9463.
12. Yang BC, Liu QY, Yao XX, Zhang DS, Dai ZC, Cui P, et al. FePt@MnO-Based Nanotheranostic Platform with Acidity-Triggered Dual-Ions Release for Enhanced MR Imaging-Guided Ferroptosis Chemodynamic Therapy. ACS Appl. Mater. Interfaces 2019; 11: 38395–38404.
13. Zhang DS, Cui P, Dai ZC, Yang BC, Yao XX, Liu QY, et al. Tumor Microenvironment Responsive FePt/MoS_2 Nanocomposites with Chemotherapy and Photothermal Therapy for Enhancing Cancer Immunotherapy. Nanoscale 2019; 11: 19912–19922.
14. Meng YF, Zhang DS, Chen X, Dai ZC, Yao XX, Cui P, et al. Nanoparticles Embedded in Metal-Organic Framework Nanoparticles for Tumor Imaging and Eradication. ACS Appl. Nano Mater. 2020; 3: 4494–4503.
15. Zhang C, Bu WB, Ni DL, Zhang SJ, Li Q, Yao ZW, et al. Synthesis of Iron Nanometallic Glasses and Their Application in Cancer Therapy by a Localized Fenton Reaction. Angew. Chem. Int. Edit. 2016; 55: 2101–2106.
16. Bayir H, Anthonymuthu TS, Tyurina YY, Patel SJ, Amoscato AA, Lamade AM, et al. Achieving Life through Death: Redox Biology of Lipid Peroxidation in Ferroptosis. Cell Chem. Biol. 2020; 27: 387–408.

17. He YJ, Liu XY, Xing L, Wan X, Chang X, Jiang HL. Fenton Reaction-Independent Ferroptosis Therapy via Glutathione and Iron Redox Couple Sequentially Triggered Lipid Peroxide Generator. Biomaterials 2020; 241: 119911.
18. Mbah NE, Lyssiotis CA. Metabolic Regulation of Ferroptosis in the Tumor Microenvironment. J. Biol. Chem. 2022; 298: 101617–101617.
19. Gulzar A, Xu JT, Wang C, He F, Yang D, Gai S, et al. Tumour Microenvironment Rresponsive Nanoconstructs for Cancer Theranostic. Nano Today 2019; 26: 16–56.
20. Wang SF, Liao HW, Li FY, Ling DS. A Mini-Review and Perspective on Ferroptosis-Inducing Strategies in Cancer Therapy. Chinese Chem. Lett. 2019; 30: 847–852.
21. Luo J, Sun M, Ritt CL, Liu X, Pei Y, Crittenden JC, et al. Tuning Pb (II) Adsorption from Aqueous Solutions on Ultrathin Iron Oxychloride (FeOCl) Nanosheets. Environ. Sci. Technol. 2019; 53: 2075–2085.
22. Yu T, Li Q, Zhao X, Xia H, Ma L, Wang J, et al. Nanoconfined Iron Oxychloride Material as a High-Performance Cathode for Rechargeable Chloride Ion Batteries. ACS Energy Lett. 2017; 2: 2341–2348.
23. Li T, He F, Liu B, Jia T, Shao B, Zhao R, et al. In Situ Synthesis of FeOCl in Hollow Dendritic Mesoporous Organosilicon for Ascorbic Acid-Enhanced and MR Imaging-Guided Chemodynamic Therapy in Neutral pH Conditions. ACS Appl. Mater. Interfaces 2020; 12: 56886–56897.
24. Qu S, Li C, Sun X, Wang J, Luo H, Wang S, et al. Enhancement of Peroxymonosulfate Activation and Utilization Efficiency *via* Iron Oxychloride Nanosheets in Visible Light. Sep. Purif. Technol. 2019; 224: 132–141.
25. Zhang J, Jiao XL, Xia YG, Liu FF, Pang YP, Zhao XF, et al. Enhanced Catalytic Activity in Liquid-Exfoliated FeOCl Nanosheets as a Fenton-Like Catalyst. Chem. Eur. J. 2016; 22: 9321–9329.
26. Zhang J, Yang M, Lian Y, Zhong M, Sha J, Liu G, et al. Ce^{3+} Self-Doped CeOx/FeOCl: An Efficient Fenton Catalyst for Phenol Degradation under Mild Conditions. Dalton T. 2019; 48: 3476–3485.
27. Rodriguez R, Schreiber SL, Conrad M. Persister Cancer Cells: Iron Addiction and Vulnerability to Ferroptosis. Mol. Cell 2022; 82: 728–740.
28. Zhou ZJ, Song JB, Tian R, Yang Z, Yu GC, Lin LS, et al. Activatable Singlet Oxygen Generation from Lipid Hydroperoxide Nanoparticles for Cancer Therapy. Angew. Chem. Int. Edit. 2017; 56: 6492–6496.
29. Wang C, Cao FJ, Ruan YD, Jia XD, Zhen WY, Jiang XE. Specific Generation of Singlet Oxygen through the Russell Mechanism in Hypoxic Tumors and GSH Depletion by Cu-TCPP Nanosheets for Cancer Therapy. Angew. Chem. Int. Edit. 2019; 58: 9846–9850.
30. Sies H. Strategies of Antioxidant Defense. Eur. J. Biochem. 1993; 215: 213–219.
31. Zhou J, Wang K, Jiang M, Li J, Yuan Y. Tumor-Acidity and Bioorthogonal Chemistry-Mediated Construction and Deconstruction of Drug Depots for Ferroptosis under Normoxia and Hypoxia. Acta Biomater. 2022; 142: 253–263.
32. Zhang L, Li G, Ouyang Z, Yang R, Gao Y, Cao X, et al. Intelligent Design of Iron-Doped LDH Nanosheets for Cooperative Chemo-Chemodynamic Therapy of Tumors. Biomater. Sci. 2022; 10:

2029–2039.

33. Chen X, Li X, Xu X, Li L, Liang N, Zhang L, et al. Ferroptosis and Cardiovascular Disease: Role of Free Radical-Induced Lipid Peroxidation. Free Radical Res. 2021; 55: 405–415.
34. Stoyanovsky DA, Tyurina YY, Shrivastava I, Bahar I, Tyurin VA, Protchenko O, et al. Iron Catalysis of Lipid Peroxidation in Ferroptosis: Regulated Enzymatic or Random Free Radical Reaction? Free Radical Bio. Med. 2019; 133: 153–161.
35. Zhao T, Guo X, Sun Y. Iron Accumulation and Lipid Peroxidation in the Aging Retina: Implication of Ferroptosis in Age-Related Macular Degeneration. Aging Dis. 2021; 12: 529–551.
36. An PJ, Gao ZG, Sun K, Gu DH, Wu H S, You CQ, et al. Photothermal-Enhanced Inactivation of Glutathione Peroxidase for Ferroptosis Sensitized by an Autophagy Promotor. ACS Appl. Mater. Interfaces 2019; 11: 42988–42997.

Schemes

Scheme 1 is available in the Supplementary Files section

Figures

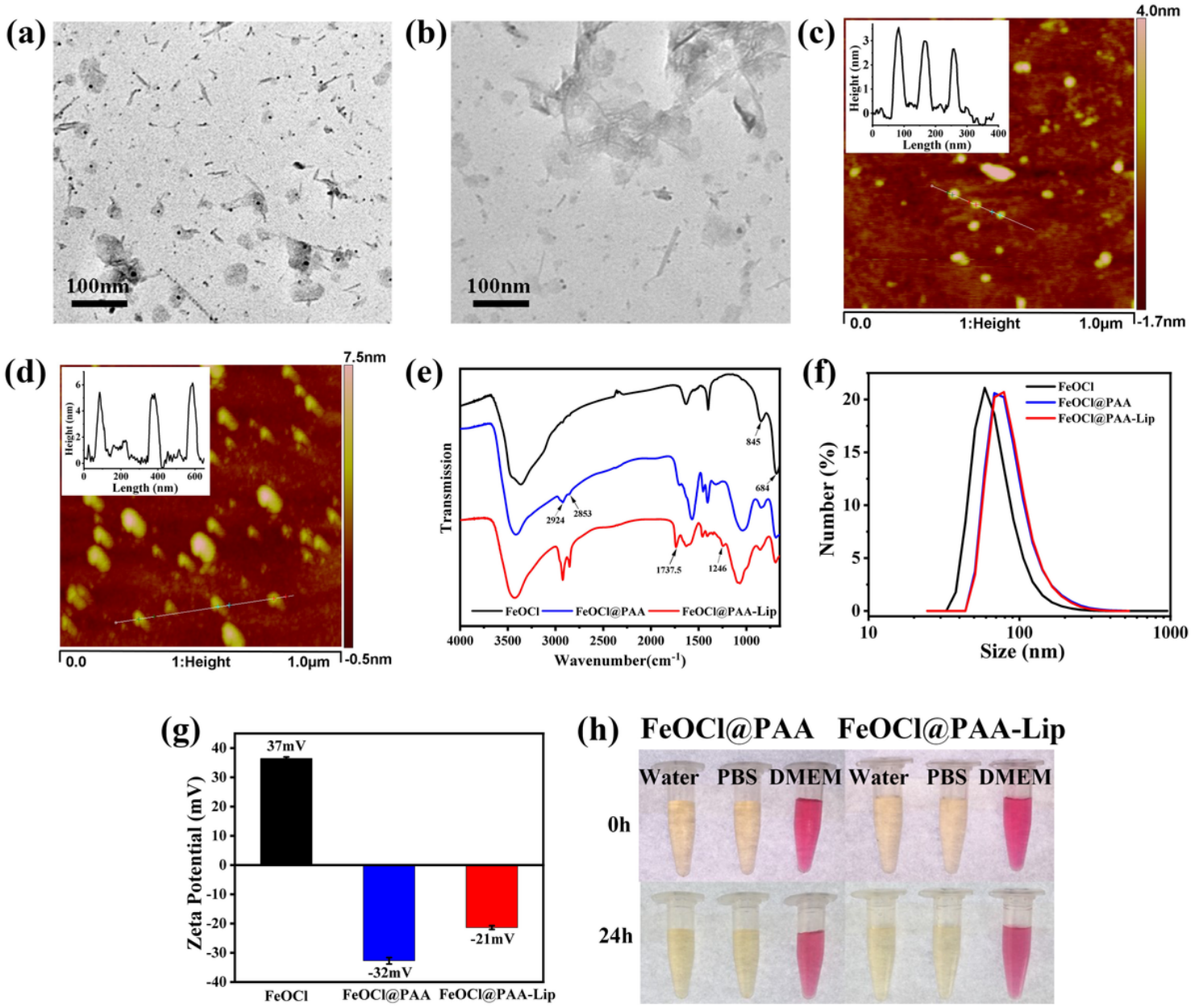

Figure 1

TEM images of FeOCl nanosheets (a) and FeOCl@PAA-Lip (b). AFM images of FeOCl nanosheets (c) and FeOCl@PAA-Lip (d). (e) FT-IR spectrum of FeOCl nanosheets, FeOCl@PAA and FeOCl@PAA-Lip. (f) Size distribution and (g) Zeta potential of FeOCl nanosheets, FeOCl@PAA and FeOCl@PAA-Lip. (h) The stability of FeOCl@PAA and FeOCl@PAA-Lip in water, PBS (pH 7.4) and DMEM at 37 °C for 24 h.

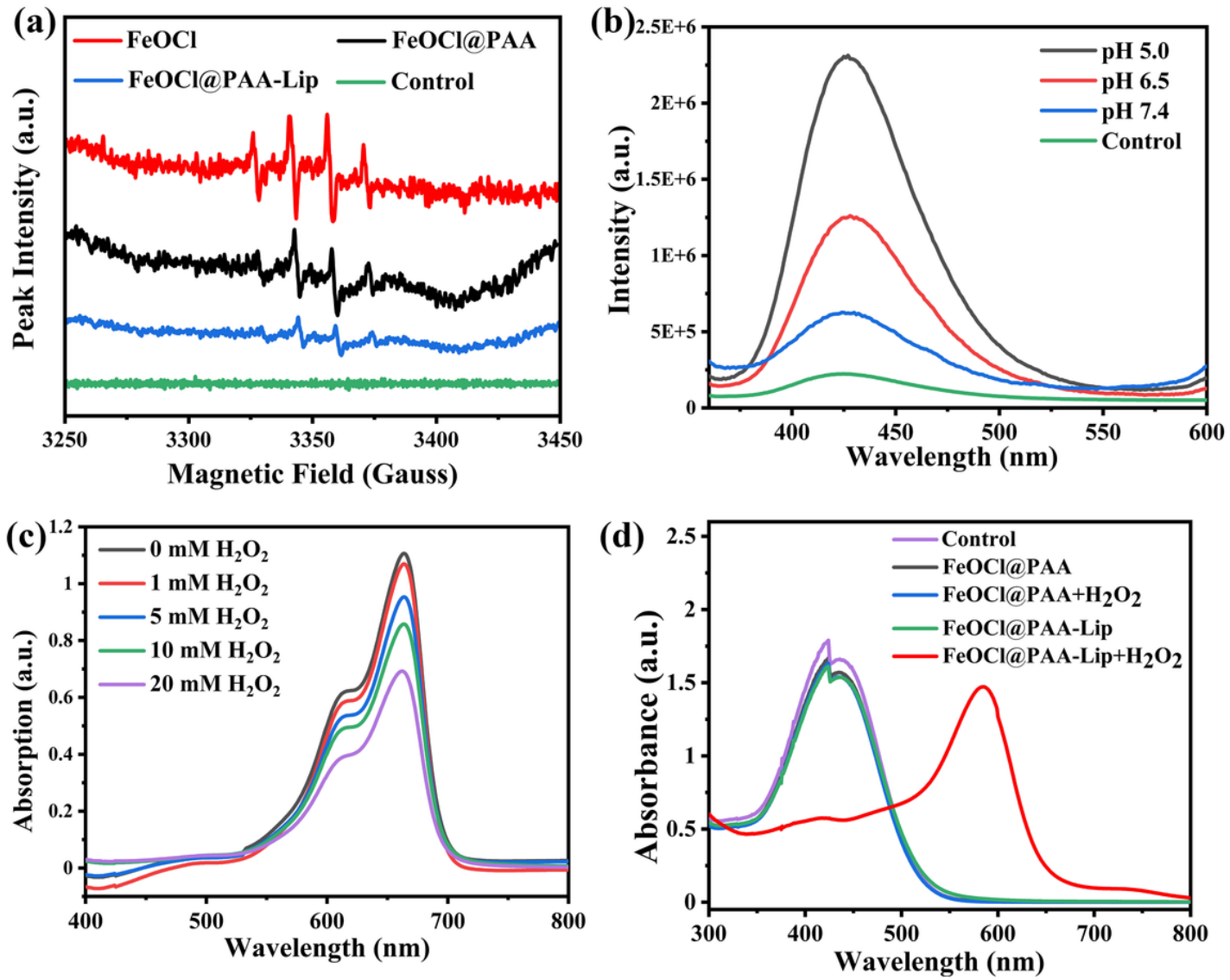

Figure 2

Production of •OH and LPO under various conditions. (a) The ESR spectra of FeOCl nanosheets, FeOCl@PAA and FeOCl@PAA-Lip at pH 7.4. (b) The TA fluorogram of FeOCl@PAA-Lip in different pH conditions. (c) The degradation curve of MB after treatment with FeOCl@PAA-Lip in various concentration of H_2O_2. (d) UV-Vis spectral of different treatment groups based on the ferrous oxidation-xylenol orange assay for LPO determination.

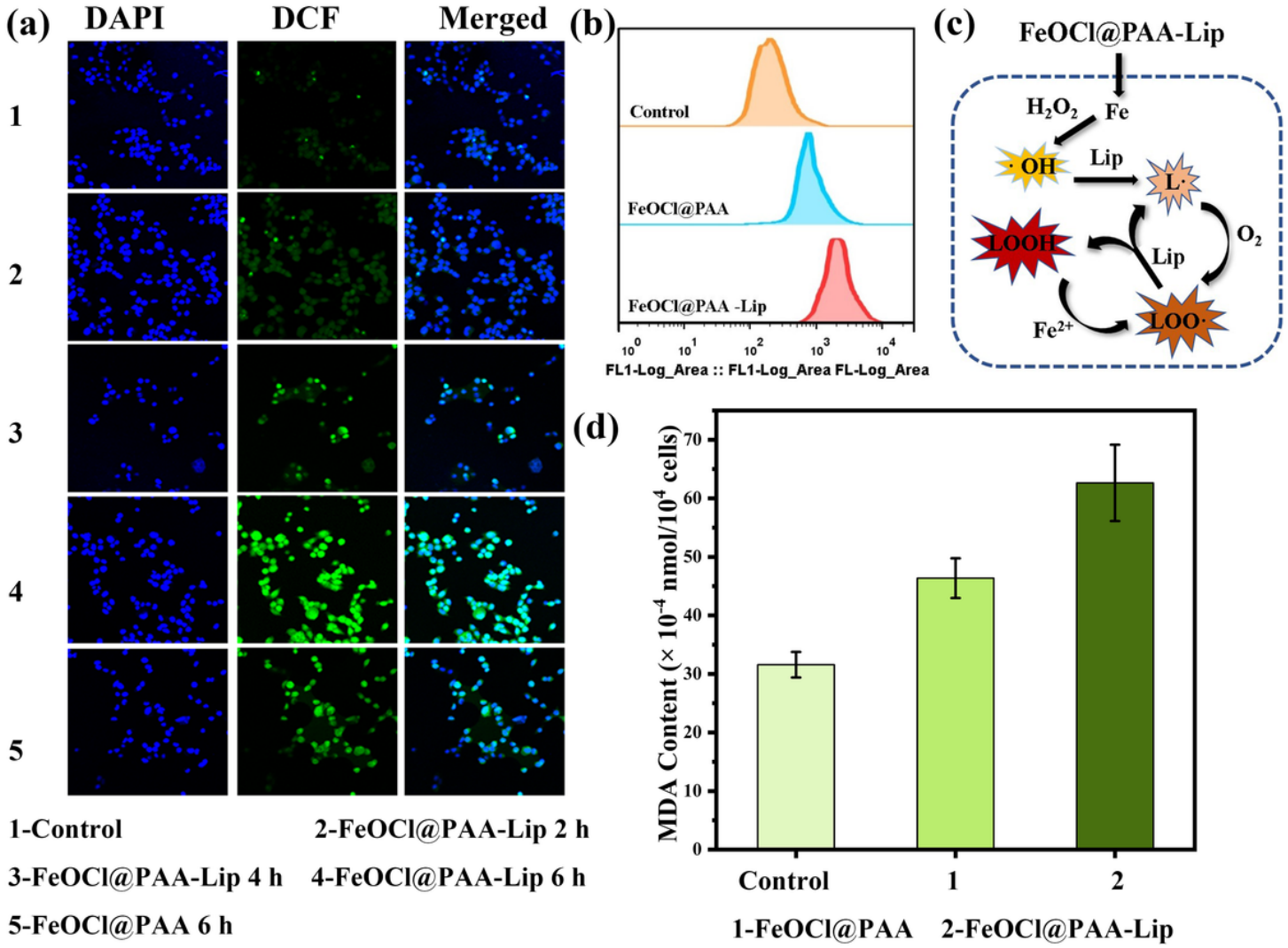

Figure 3

FeOCl@PAA-Lip triggers the cascade generation of intracellular ROS and LPO in cancer cells. (a) CLSM images of DCFH-DA labeled 4T1 cells incubated with FeOCl@PAA and FeOCl@PAA-Lip. (b) Flow cytometry of 4T1 cells after 6 h treated with FeOCl@PAA and FeOCl@PAA-Lip. (c) Schematic illustration of lipid peroxidation in tumor cells treated with FeOCl@PAA-Lip. (d) Detection of the LPO level in 4T1 cells treated with FeOCl@PAA and FeOCl@PAA-Lip by MDA assay kit.

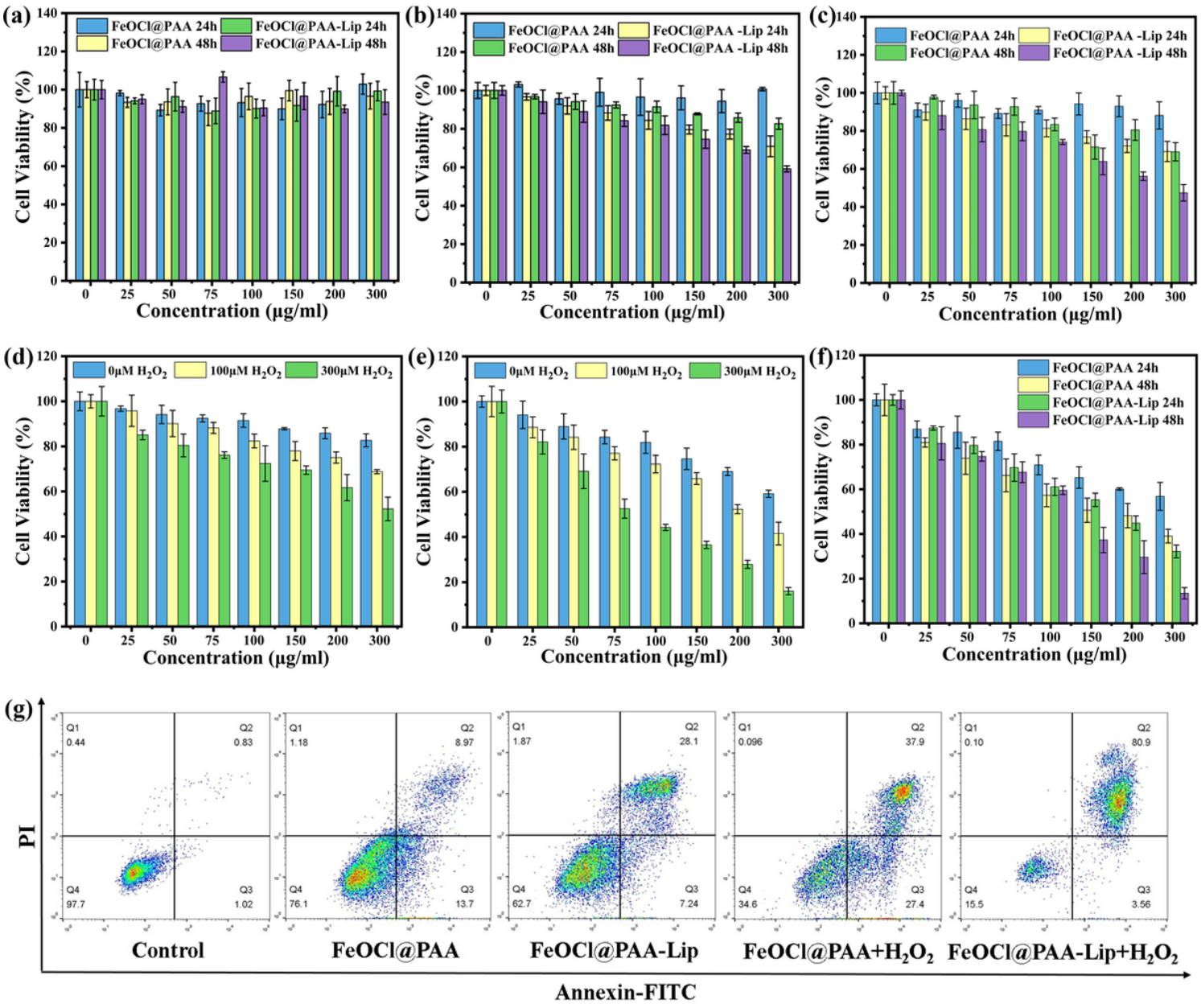

Figure 4

Cell viability of L929 cells (a), 4T1 cells (b) and U87 cells (c) after 24 h and 48 h of incubation with FeOCl@PAA and FeOCl@PAA-Lip. Cell viability of 4T1 cells treated with FeOCl@PAA (d) and FeOCl@PAA-Lip (e) with different H_2O_2 concentration. (f) Cell viability of U87 cells treated with FeOCl@PAA and FeOCl@PAA-Lip containing 300 μM H_2O_2. (g) Determination of apoptosis in 4T1 cells by flow cytometry after various treatments.

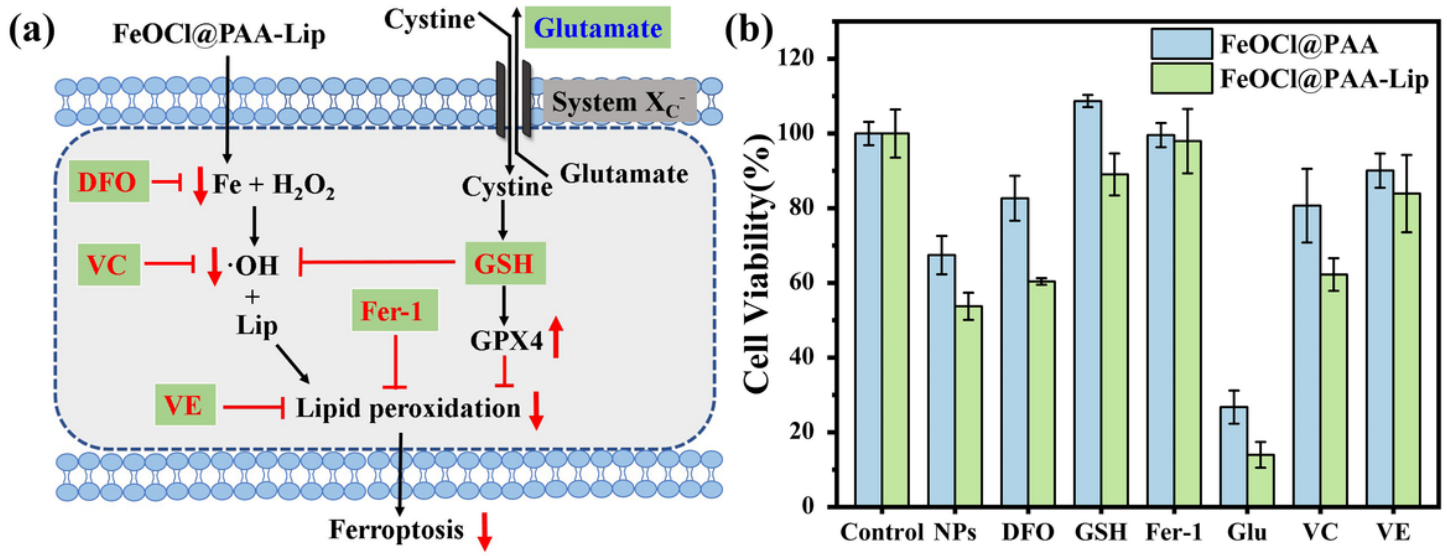

Figure 5

(a) Schematic illustration of ferroptosis induced by FeOCl@PAA-Lip and ferroptosis-related compounds. (b) Cell viability of 4T1 cells treated with FeOCl@PAA and FeOCl@PAA-Lip with the addition of DFO, GSH, Fer-1, Glu, VC and VE, respectively.

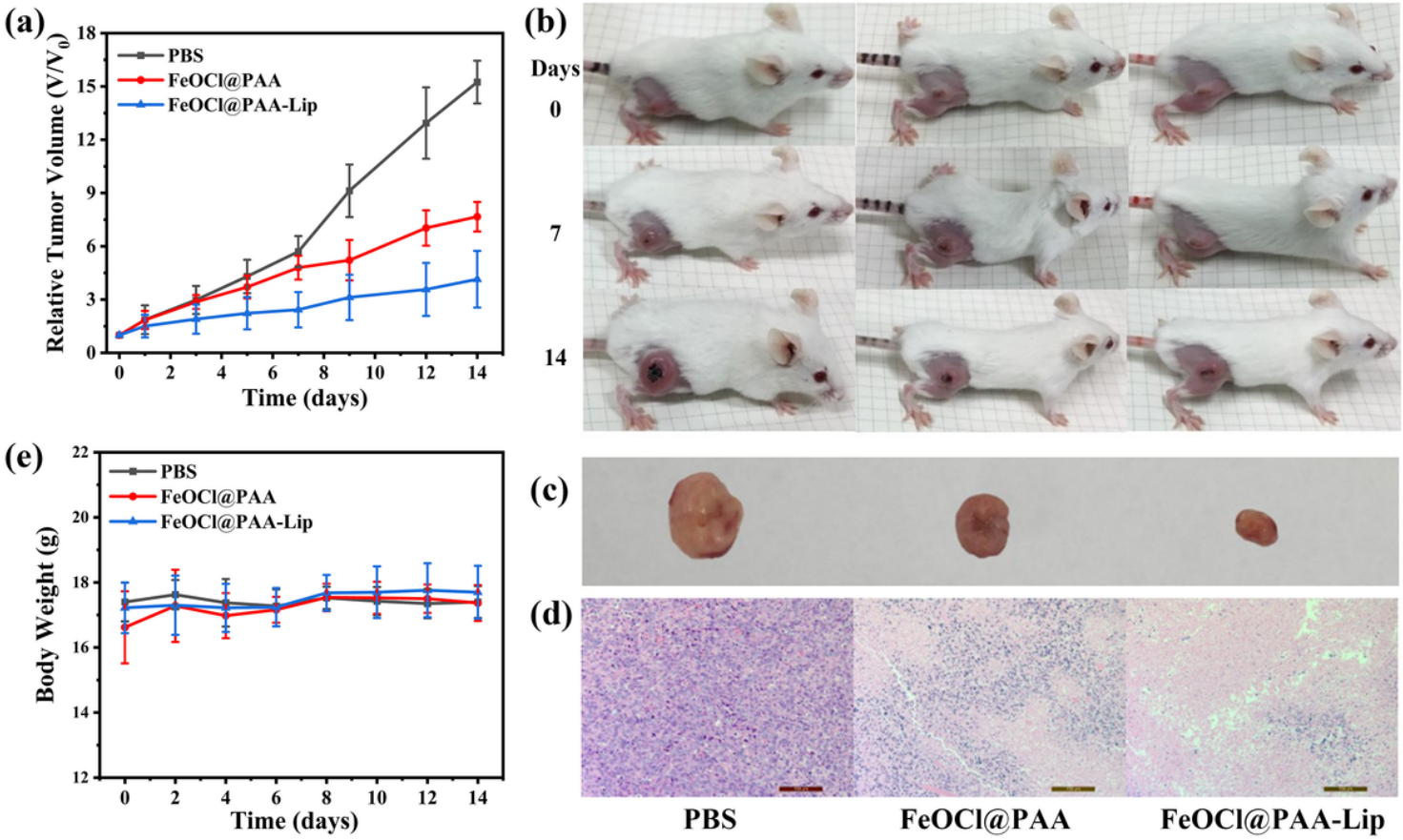

Figure 6

In vivo anti-tumor effect. (a) Variation of relative tumor volume of the mice treated with PBS, FeOCl@PAA and FeOCl@PAA-Lip during 14 days. (b) The digital photographs of mice in all three groups at day 0, day 7 and day 14 under various treatments. (c) Photographs and (d) H&E stained images of tumors after various treatments for 14 days. (e) Variation of average weight of the mice treated with PBS, FeOCl@PAA and FeOCl@PAA-Lip.

Figure 7

(a) The hemolysis rate of FeOCl@PAA-Lip in fresh blood at different concentrations. (b) *In vivo* fluorescence imaging of tumor-bearing mice after intravenous injection of Cy5.5/FeOCl@PAA-Lip (left) and free Cy 5.5 (right) at different time. (c) Iron content of various organs harvested from tumor-bearing mice after intravenous injection of PBS, FeOCl@PAA and FeOCl@PAA-Lip after 24 h.

Supplementary Files

This is a list of supplementary files associated with this preprint. Click to download.

- Scheme1.png
- SupportingInformation.docx